Materials Advances

ROYAL SOCIETY OF CHEMISTRY

COMMUNICATION

View Article Online
View Journal | View Issue

Check for updates

Cite this: *Mater. Adv.*, 2024, 5, 1892

Received 30th November 2023,
Accepted 3rd February 2024

DOI: 10.1039/d3ma01070h

rsc.li/materials-advances

A defective NiCo-pentlandite/black phosphorus heterostructure for efficient water splitting electrocatalysis†

Hang Liu,‡[a] Yahui Tian,‡[b] Syama Lenus,[a] Xin Zhao,[a] Zhengfei Dai[a] and Tingting Liang*[ac]

Herein, we report a nickel cobalt pentlandite/black phosphorus (Ni–Co_9S_8/BP) heterostructure as a bifunctional electrocatalyst, *i.e.*, Ni doped Co_9S_8 vertically grown on the surface of black phosphorus. The nanoporous network heterostructure and surface sulfur vacancies endow Ni–Co_9S_8/BP with more active sites and accelerated reaction kinetics, thus realizing a low potential of 1.65 V at 10 mA cm^{-2} for water splitting, which outperforms most Co_9S_8-based electrocatalysts.

Electrochemical water electrolysis (EWS) is considered as a promising, environmentally friendly, and effective approach to generate hydrogen with high purity, which consists of the hydrogen evolution reaction (HER) at the cathode and the oxygen evolution reaction (OER) at the anode.[1–3] In the past few decades, noble metal-based materials (*e.g.*, Pt-based ones for the HER and Ir- or Ru-based ones for the OER) are widely regarded as activity references for EWS, but these catalysts suffer from their scarcity and limited sustainability for large-scale production.[4,5] Hence, developing earth-abundant and non-precious transition metal-based catalysts as alternatives is of great importance for the widespread commercialization and renewable acceleration of hydrogen energy.[6–8] Among a great number of transition metal-based catalysts, transition metal sulphide (TMS) compounds have aroused tremendous attention due to their variant 3d-valence electrons and favourable electrical conductivity for boosting the HER and OER processes.[9–12] In this case, nanostructured cobalt sulphides are emerging as appealing bifunctional electrocatalysts for EWS by virtue of their excellent catalytic properties (*e.g.*, low water dissociation energy and enriched active sites) and remarkable electrochemical stability.[13–16] For example, Ma *et al.* synthesized Co_9S_8 hollow spheres (HSs) as bifunctional catalysts with low overpotentials of 267 mV (HER) and 342 mV (OER) at a current density of 10 mA cm^{-2} in alkaline electrolyte.[17] Despite much progress having been achieved so far, further improvement in the electrocatalytic properties of cobalt sulphides is still very demanded.

An applicable strategy is cation valence engineering through metal heteroatom doping.[2,18] The existence of metal heteroatoms at the interface of the electrocatalyst can enhance the intrinsic electrocatalytic activity by tuning the surface electronic states and the electron donating/accepting behaviors.[6,19] A recent work demonstrated that the prepared Co_3S_4 nanowires with doping a small amount of Ni show a lower HER overpotential of 199 mV at 10 mA cm^{-2} when compared to pristine Co_3S_4 (218 mV at 10 mA cm^{-2}).[18] Another practical strategy to improve the EWS performance is the intrinsic defect construction on the nanostructured cobalt sulphide.[20,21] It has been proven that the S vacancy (V_s) is capable of promoting the electron mobility and maximizing the active sites due to the low number of coordination bonds.[22–24] Zhu *et al.* reported that $CoS_{0.61}Se_{0.25}$ HSs with V_s were synthesized by Se heteroatom substitution, in which a low overpotential of 108 mV at 10 mA cm^{-2} for the HER was delivered.[24] Besides, a rapid interfacial charge transfer over electrocatalysts is also elementary for an efficient EWS process.[25] Hybridizing active catalysts with other conductive materials is normally noticed as a beneficial route to promote the EWS performance.[26–30] Owing to their unique electronic characteristics (*e.g.*, a high carrier mobility of ~1000 cm^2 V^{-1} s^{-1}, adjustable bandgap, *etc.*) and high hydrophilicity, p-type black phosphorus (BP) lamellae can be promising conductive candidates to host cobalt sulphide-based catalysts, since the injection effect of oxidative holes would further facilitate the OER process.[25,31] Bearing the above-mentioned strategies in mind, it is thus expected that designing BP-hosted cobalt sulphide coupled with metal doping and S vacancies as the

[a] State Key Laboratory for Mechanical Behavior of Materials, Xi'an Jiaotong University, Xi'an 710049, China. E-mail: liangtingting@haust.edu.can
[b] Institute of Physical Science and Information Technology, Anhui University, Hefei, 230601, China
[c] School of Materials Science and Engineering, Henan University of Science and Technology, Luoyang, 471023, China

† Electronic supplementary information (ESI) available. See DOI: https://doi.org/10.1039/d3ma01070h

‡ These authors contributed equally to this work.

bifunctional water splitting electrocatalyst can be an appropriate option for high-performance EWS.

In this communication, we have fabricated a NiCo-pentlandite/black phosphorus heterostructure (Ni–Co_9S_8/BP) with S vacancies to realize highly active and durable water electrolysis. For the preparation of Ni–Co_9S_8/BP, NiCo hydroxide nanosheets were initially grown *in situ* vertically on few-layer BP, followed by one-step sulfurization. The as-prepared nanostructured heterostructure exhibits excellent electrocatalytic performance for both alkaline HER and OER with small overpotentials (η_{10}, at 10 mA cm^{-2}) of 160 mV and 258 mV, respectively. The water electrolyser assembled with Ni–Co_9S_8/BP displays a low potential of 1.65 V at 10 mA cm^{-2} with long-term stability. The experimental investigations of the Ni–Co_9S_8/BP heterostructure have unveiled that, compared to its counterparts, the increased ratio of Ni^{3+}/Ni^{2+} and the generated S vacancies play electron-accepting roles, and the reduced ratio of Co^{3+}/Co^{2+} possesses the electron-donating character for promoting the OER and HER processes, respectively. Research sheds light on valence engineering and vacancy modulation in BP-based heterostructure electrocatalysts.

The synthesis process of the Ni–Co_9S_8/BP heterostructure is shown in Fig. 1a. The bulk BP crystal was first electro-exfoliated into BP lamellae *via* a two-electrode equipment in an electrolyte, as we previously reported.[6,32] Then, Ni–$Co(OH)_2$ was loaded on the BP lamellae to form the interface of Ni–$Co(OH)_2$/BP through the wet-chemical synthesis and subsequent annealing process, which was determined by XRD after comparison with the standard diffraction patterns (Fig. S1a, ESI†). The SEM (Fig. 1b) and TEM images (Fig. S1b and c, ESI†) of Ni–$Co(OH)_2$/BP both confirm that Ni–$Co(OH)_2$ nanosheets grow vertically on the BP lamellae, forming a nanoporous network heterostructure. The as-prepared Ni–$Co(OH)_2$/BP was finally forwarded to the Ni–Co_9S_8/BP heterostructure by one-step sulfurization. The SEM and TEM images of Ni–Co_9S_8/BP show that the as-formed heterostructure still maintains the porous morphology as displayed in Fig. 1c and Fig. S2a (ESI†), which could possibly benefit gas dissipation and exposure of the active-edge sites of Ni–Co_9S_8 for promoting the water-electrolytic kinetic process. The HRTEM image of Ni–Co_9S_8/BP is also displayed in Fig. 1d. It illustrates lattice fringes with spacings of 0.525 nm and 0.286 nm, corresponding to the (020) plane of BP and the (222) plane of Co_9S_8, respectively. Furthermore, the SAED images in Fig. 1e indicate the (040) lattice plane of BP and the (111)/(420) planes of Co_9S_8, respectively. The elemental mappings (Fig. S2b, ESI†) confirm the uniform distributions of P, Co, Ni and S in the Ni–Co_9S_8/BP heterostructure. Fig. 1f presents the XRD pattern of the Ni–Co_9S_8/BP heterostructure along with that of Co_9S_8/BP. The main peaks of Ni–Co_9S_8/BP located at 29.67°, 31.06°, 47.89° and 51.97° correspond to the (311), (222), (511) and (440) crystal planes of Co_9S_8 (JCPDS No. 86-2273).[33] The other peaks of Ni–Co_9S_8/BP at 33.87° and 35.00° are in accordance with the (040) and (111) planes of BP (JCPDS No. 73-1358).[34] As for references, the SEM images of $Co(OH)_2$, Ni–$Co(OH)_2$, $Co(OH)_2$/BP, Co_9S_8, Ni–Co_9S_8, and Co_9S_8/BP are also provided in Fig. S3 (ESI†).

Afterwards, the chemical valence and compositions of different samples were investigated by XPS as shown in Fig. 2a–c and Fig. S4 (ESI†). The deconvolution of Co 2p XPS spectra is displayed in Fig. 2a. Two sets of doublets are assigned to Co $2p_{3/2}$ (779 eV, Co^{3+}; 781.5 eV, Co^{2+}) and Co $2p_{1/2}$ (794.1 eV, Co^{3+}; 797.4 eV, Co^{2+}), respectively.[35] The Ni 2p XPS spectra in Fig. 2b show that two sets of doublets correspond to Ni $2p_{3/2}$ (854.2 eV,

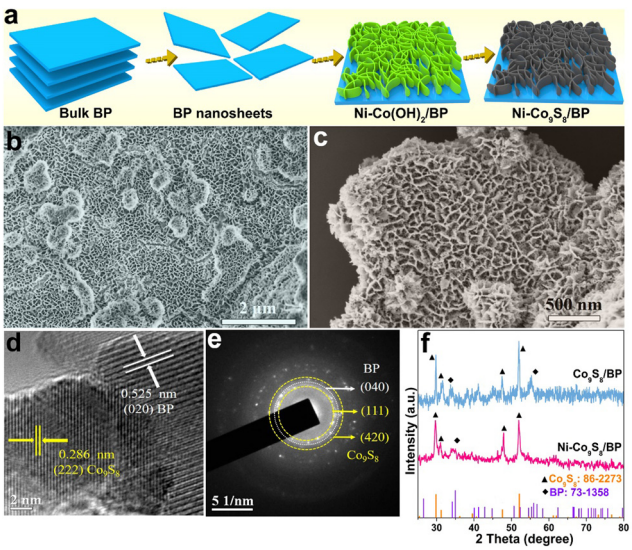

Fig. 1 (a) Synthesis diagram of the Ni–Co_9S_8/BP heterostructure. SEM images of (b) Ni–$Co(OH)_2$/BP and (c) Ni–Co_9S_8/BP. (d) HRTEM and (e) SAED images of Ni–Co_9S_8/BP. (f) XRD patterns of Co_9S_8/BP and Ni–Co_9S_8/BP, respectively.

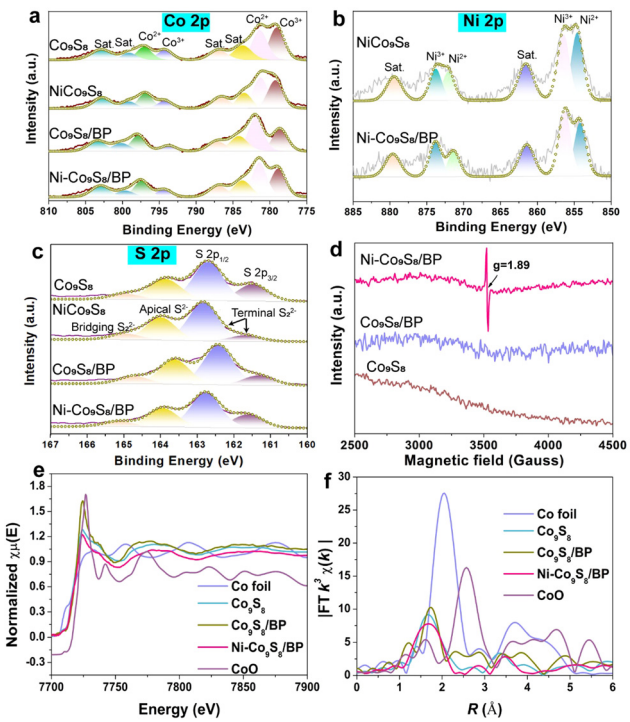

Fig. 2 (a)–(c) High-resolution Co 2p, Ni 2p and S 2p XPS spectra of the relevant samples. (d) EPR spectra of Co_9S_8, Ni–Co_9S_8, and Co_9S_8/BP, respectively. (e) XANES and (f) EXAFS spectra of Co, CoO, Co_9S_8, Co_9S_8/BP and Ni–Co_9S_8/BP, respectively.

Ni^{2+}; 856.4 eV, Ni^{3+}) and Ni $2p_{1/2}$ (871.2 eV, Ni^{2+}; 873.8 eV, Ni^{3+}).[36] It is revealed that the valence states of Ni–Co_9S_8/BP are reconstructed due to the increased ratio of Ni^{3+}/Ni^{2+} and the reduced ratio of Co^{3+}/Co^{2+} after Ni doping and BP hosting, undertaking both electron-accepting and electron-donating characters for enhancing the HER and OER. The S 2p spectra in Fig. 2c present S $2p_{1/2}$ (162.7 eV), S $2p_{3/2}$ (161.5 eV), apical S^{2-} (163.9 eV) and bridging S_2^{2-} (165 eV).[6] The P 2p spectra in Fig. S4b (ESI†) shows that a set of doublets located in the range of ~128–132 eV are regarded to P $2p_{3/2}$ and P $2p_{1/2}$, respectively.[6] A peak at a higher binding energy is generally considered as P–O bonding.[34] When compared to Co_9S_8 and Co_9S_8/BP, the EPR signal intensity of Ni–Co_9S_8/BP can be observed at a *g*-factor of 1.89, which is attributed to the presence of V_s upon Ni doping (Fig. 2d).[37] Thus, it can be deduced that the nanoscale Kirkendall effect takes place in the transformation of Ni–$Co(OH)_2$/BP to Ni–Co_9S_8/BP during the subsequent sulfurization process.[38] The unbalanced diffusion rates between the rapid outward diffusion of the Ni atom from the Ni–$Co(OH)_2$ nanosheet and the slow inward pervasion of S atoms from sulphur powder result in V_s formation within the nanosheet. The V_s with a high electron-accepting capacity can be also regarded as active sites for the OER.[39]

Besides, the surface area and pore structure of the Ni–Co_9S_8/BP sample were studied based on the N_2 adsorption/desorption isotherms, as shown in Fig. S5 (ESI†). It gives a type-IV isotherm with a typical H3-type hysteresis loop, demonstrating a mesoporous structure.[40,41] Ni–Co_9S_8/BP has a high BET specific surface area of 153.18 $m^2\ g^{-1}$, which is much higher than those of the other representative reference samples (*e.g.*, Ni–Co_9S_8, 15.90 $m^2\ g^{-1}$; Ni–$Co(OH)_2$/BP, 19.41 $m^2\ g^{-1}$; Ni–$Co(OH)_2$, 3.64 $m^2\ g^{-1}$). The high BET surface area of Ni–Co_9S_8/BP is further capable of boosting its electrocatalytic activity since more active sites are exposed during the catalytic reactions.[42] The coordination environment and chemical state of Ni–Co_9S_8/BP were then investigated by XANES and EXAFS spectroscopies. Fig. 2e shows the Co K-edge XANES spectra of the relevant samples. Compared to Co_9S_8 and Co_9S_8/BP, the Co K-edge spectrum of Ni–Co_9S_8/BP has a gradual shift to lower energies, confirming the change in the Co state from Co^{3+} to Co^{2+}.[39] The position of the absorption edge for Ni–Co_9S_8/BP is between Co foil and Co_9S_8/BP, much closer to Co_9S_8/BP. Therefore, this characteristic indicates Co^{2+} is the major valence state of Co in Ni–Co_9S_8/BP, which is well consistent with the XPS analyses in Fig. 2a.[43] In Fig. 2f, the Co K-edge Fourier-transform (FT) EXAFS spectrum of Ni–Co_9S_8/BP displays a peak at ~1.69 Å, which corresponds to the Co–S bonding environment. Compared to the peak at 1.72 Å in the spectrum of Co_9S_8/BP, the lower value of Ni–Co_9S_8/BP indicates the shorter electron-transfer path in Ni–Co_9S_8/BP.[44]

To investigate the HER electrocatalytic properties, LSV curves were tested after 50 cycles of stabilization (Fig. 3a). Ni–Co_9S_8/BP shows a η_{10} overpotential of 121 mV in 0.5 M H_2SO_4, which is much lower than those of Co_9S_8/BP (202 mV), Ni–Co_9S_8 (218 mV), Co_9S_8 (218 mV) and BP (403 mV). The corresponding Tafel slopes were calculated and are presented in Fig. S6a (ESI†), where all the Tafel slopes of the catalysts, except for BP, are

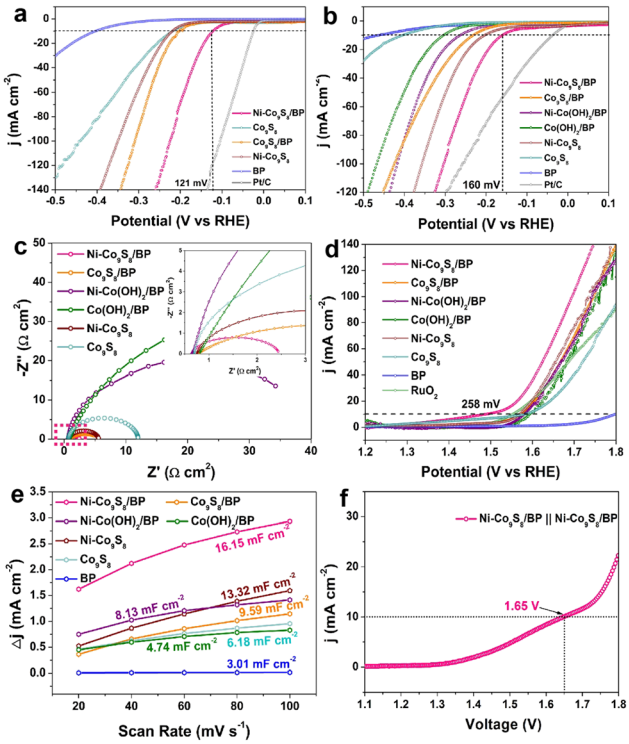

Fig. 3 HER polarization curves of relevant samples in (a) 0.5 M H_2SO_4 and (b) 1 M KOH, respectively. (c) EIS spectra (the inset shows the enlarged area of the pink dotted line). (d) OER polarization curves of relevant samples in 1 M KOH. (e) Current–potential curves with different scan rates in 1 M KOH. (f) Polarization curves of overall water splitting based on the Ni–Co_9S_8/BP‖Ni–Co_9S_8/BP couple.

lower than 118 mV dec^{-1}, indicating the rate-determining step (RDS) during the HER process is the Volmer step ($H_3O^+ + e^- \rightarrow H_{ads}$).[6] Specifically, the Tafel slope for Ni–Co_9S_8/BP (76 mV dec^{-1}) is smaller than the values for Co_9S_8/BP (91 mV dec^{-1}), Ni–Co_9S_8 (101 mV dec^{-1}) and Co_9S_8 (101 mV dec^{-1}), illustrating that Ni–Co_9S_8/BP has the most favourable HER kinetics over the other reference electrocatalysts. The HER performance of Ni–Co_9S_8/BP in 1 M KOH was also measured and is shown in Fig. 3b and Fig. S6b (ESI†). The comparison of the reference samples and Ni–Co_9S_8/BP reveals a higher HER catalytic activity for the latter, featuring a smaller η_{10} overpotential of 160 mV and a smaller Tafel slope of 119 mV dec^{-1}. The values of η_{10} overpotentials and Tafel slopes found here are comparable or superior to those of the reported relevant catalysts in acidic and basic media (Table S1, ESI†). The electrochemical impedance spectroscopy (EIS) measurements further give additional insights into HER kinetics and interfacial properties (Fig. 3c). Nyquist plots show that Ni–Co_9S_8/BP has the smallest charge-transfer resistance among all the samples, which is in agreement with the superior catalytic activity of Ni–Co_9S_8/BP examined by LSV. To estimate the stability of Ni–Co_9S_8/BP, the chronopotentiometry tests were performed in both 1 M KOH and 0.5 M H_2SO_4, as shown in Fig. S6c and d (ESI†). The HER catalytic currents are sustainable with slight fluctuations after 24 h, indicating a high stability in both acidic and basic media.

The OER catalytic performance was also tested in 1 M KOH after 50 cycles of stabilization. Fig. 3d shows the LSV curves of

the samples, illustrating the catalytic properties of Ni–Co_9S_8/BP with a η_{10} overpotential of 258 mV, which is much lower than those of commercial RuO_2 (322 mV), Co_9S_8/BP (341 mV), Ni–$Co(OH)_2$/BP (351 mV), $Co(OH)_2$/BP (363 mV), Ni–Co_9S_8 (340 mV) and Co_9S_8 (352 mV). The η_{10} overpotential for Ni–Co_9S_8/BP is striking as compared to the other relevant OER catalysts listed in Table S2 (ESI†). In Fig. S6e (ESI†), analysis of the data gives a Tafel value of 118 mV dec^{-1} for Ni–Co_9S_8/BP. To estimate the electrochemically active surface area (ECSA), the electrochemical double-layer capacitance (C_{dl}) at the solid–liquid interface was obtained through CV measurements at various scan rates (Fig. S7, ESI†). Compared to the other reference samples, the C_{dl} for Ni–Co_9S_8/BP shows a considerable increase with a value of 16.15 mF cm^{-2} (Fig. 3e), suggesting the higher ECSA for the OER. As presented in Fig. S6f (ESI†), the chronopotentiometry measurement for Ni–Co_9S_8/BP was then carried out for 24 h, illustrating the good retention of OER catalytic activity. The structural characterization after the OER stability test was also checked and is shown in Fig. S8 (ESI†). The morphology of lamellae is well preserved and Ni–Co_9S_8/BP maintains its phases of Co_9S_8 and BP. The EDX maps confirm the elements of Ni–Co_9S_8/BP remain well after the OER stability test. Given its capabilities for both water oxidation and reduction, the Ni–Co_9S_8/BP catalysts were investigated for their overall water splitting (OWS) performance in 1.0 M KOH with a two-electrode setup. In order to achieve a water splitting current density of 10 mA cm^{-2}, a cell voltage of 1.65 V was needed for Ni–Co_9S_8/BP‖Ni–Co_9S_8/BP electrolysers, as shown in Fig. 3f. As a bifunctional electrocatalyst, the performance of Ni–Co_9S_8/BP for OWS is superior to the results reported for relevant bifunctional electrocatalysts (Table S3, ESI†). The durability of the Ni–Co_9S_8/BP‖Ni–Co_9S_8/BP electrolysers was examined in the long-term electrolysis experiment at a cell voltage of 1.65 V in 1.0 M KOH (Fig. S6g, ESI†). The water splitting current remained almost constant with only a slight degradation by the end of the electrolysis.

In summary, we have successfully developed a nickel-doped cobalt sulphide/black phosphorus heterostructure by growing NiCo hydroxide nanosheets on BP lamellae and subsequent one-step sulfurization for electrochemical water electrolysis. Based on the above-mentioned evidence, not only Ni^{3+}/Ni^{2+} and Co^{3+}/Co^{2+} pairs have been reconstructed, but also S vacancies have been generated after Ni doping and BP hosting in Ni–Co_9S_8/BP. The modulated Ni^{3+}/Ni^{2+} and S vacancies play electron-accepting roles, while the tuned Co^{3+}/Co^{2+} exhibits the electron-donating character for boosting the water splitting process. Thanks to the hetero-interface engineering and dual-modulation strategy (*i.e.*, Ni doping and S vacancy modulation), the as-synthesized Ni–Co_9S_8/BP heterostructure exhibits excellent electrocatalytic performance for both the HER (η_{10} overpotentials of 121 mV in 0.5 M H_2SO_4 and 160 mV in 1 M KOH) and OER (η_{10} overpotential of 258 mV in 1 M KOH). A two-electrode electrolyser with Ni–Co_9S_8/BP catalysts only needs 1.65 V at 10 mA cm^{-2} for stable overall water splitting. This work opens a new avenue for designing advanced noble-metal-free electrocatalysts by co-engineering the interface and electronic structure.

Conflicts of interest

There are no conflicts to declare.

Acknowledgements

This work was jointly supported by the National Natural Science Foundation of China (Grant No. 62304177 and 52003216), the Postdoctoral Science Foundation of China (2021M692546 and 2022M710045), the Key Scientific Research Project of Colleges and Universities in Henan Province (23A430031), and the Key Research and Development Program of Shaanxi (2023-YBSF-150).

Notes and references

1 F. J. Qin, D. N. Zhou, M. R. Sun, W. J. Xu, H. Tang, J. L. Fan and W. X. Chen, *Chem. Commun.*, 2021, **57**, 11561–11564.
2 W. Y. An, H. Lee, S. R. Choi, S. Choi, H.-S. Cho, M. Choi and J.-Y. Park, *J. Mater. Chem. A*, 2023, **11**, 5734–5745.
3 T. Zhu, B. Wu, J. Xie, H. R. Yang, W. B. Zhang and Y. Y. Sun, *ACS Sustainable Chem. Eng.*, 2023, **11**, 17482–17491.
4 J. N. Song, S. Zhao, D. Liu, Y. X. Xiong, F. Hu, L. L. Li, L. Li, H. Pan and S. J. Peng, *Chem. Commun.*, 2022, **58**, 9662–9665.
5 M. J. Luo, T. Wu, S. M. Xu, R. Q. Wang and F. Q. Huang, *Chem. Commun.*, 2022, **58**, 6204–6207.
6 T. T. Liang, S. Lenus, Y. D. Liu, Y. Chen, T. Sakthivel, F. Y. Chen, F. Ma and Z. F. Dai, *Energy Environ. Mater.*, 2023, e12332.
7 S. J. Shen, Z. P. Wang, Z. P. Lin, K. Song, Q. H. Zhang, F. Q. Meng, L. Gu and W. W. Zhong, *Adv. Mater.*, 2022, **34**, 2110631.
8 S. Banerjee, A. Kakekhani, R. B. Wexler and A. M. Rappe, *ACS Catal.*, 2023, **13**, 4611–4621.
9 H. Su, J. Jiang, S. J. Song, B. H. An, N. Li, Y. Q. Gao and L. Ge, *Chin. J. Catal.*, 2023, **44**, 7–49.
10 J. M. Zhu, S. J. Zi, N. Zhang, Y. Hu, L. An and P. X. Xi, *Small*, 2023, 2301762.
11 S. Roy, W. Choi, S. Jeon, D.-H. Kim, H. Kim, S. J. Yun, Y. Lee, J. Lee, Y.-M. Kim and J. Kim, *Nano Lett.*, 2018, **18**, 4523–4530.
12 W. X. Chen, Y. J. Hu, P. Peng, J. H. Cui, J. M. Wang, W. Wei, Y. Y. Zhang, K. K. Ostrikov and S.-Q. Zang, *Sci. China Mater.*, 2022, **65**, 2421–2432.
13 S. Chakrabartty, S. Karmakar and C. R. Raj, *ACS Appl. Nano Mater.*, 2020, **3**, 11326–11334.
14 S. J. Deng, Y. Zhong, Y. X. Zeng, Y. D. Wang, X. L. Wang, X. H. Lu, X. H. Xia and J. P. Tu, *Adv. Sci.*, 2018, **5**, 1700772.
15 L. L. Feng, G. D. Li, Y. Liu, Y. Wu, H. Chen, Y. Wang, Y. C. Zou, D. Wang and X. Zou, *ACS Appl. Mater. Interfaces*, 2015, **7**, 980–988.
16 J. Yu, Z. Li, T. Liu, S. Y. Zhao, D. Q. Guan, D. F. Chen, Z. P. Shao and M. Ni, *Chem. Eng. J.*, 2023, **460**, 141674.
17 X. Y. Ma, W. Zhang, Y. D. Deng, C. Zhong, W. B. Hu and X. P. Han, *Nanoscale*, 2018, **10**, 4816–4824.
18 S. S. Tang, X. Wang, Y. Q. Zhang, M. Courté, H. J. Fan and F. Denis, *Nanoscale*, 2019, **11**, 2202–2210.

19 X. W. Zhang, Y. Y. Liu, J. Gao, G. S. Han, M. F. Hu, X. L. Wu, H. Q. Cao, X. Y. Wang and B. J. Li, *J. Mater. Chem. A*, 2018, **6**, 7977–7987.
20 Y. Yang, D. R. Wang, Y. Y. Wang, Z. L. Li, R. Su, X. Wang, T. Xu and S. X. Wang, *ACS Appl. Energy Mater.*, 2022, **5**, 14869–14880.
21 T. C. Khiem, N. N. Huy, E. Kwon, X. G. Duan, S. Wacławek, J. Bedia, Y. C. Tsai, A. Ebrahimi, F. Ghanbari and K.-Y. Lin, *Appl. Catal., B*, 2023, **330**, 122550.
22 M. J. Liu, L. Wang, X. Y. Yu, H. Zhang, H. Zhang, S. K. Li and F. Z. Huang, *Energy*, 2022, **238**, 121767.
23 F. Wu, R. Yang, S. S. Lu, W. Du, B. Zhang and Y. M. Shi, *ACS Energy Lett.*, 2022, **7**, 4198–4203.
24 T. Zhu, Y. Xiao, Y. F. Ren, W. Zeng, A. Q. Pan, Y. Y. Zheng and Q. B. Liu, *ACS Appl. Energy Mater.*, 2021, **4**, 2976–2982.
25 W. F. Zhai, Y. Chen, Y. D. Liu, T. Sakthivel, Y. Y. Ma, Y. B. Qin, Y. Q. Qu and Z. F. Dai, *ACS Nano*, 2023, **17**, 17254–17264.
26 H. Liu, A. Zakhtser, A. Naitabdi, F. Rochet, F. Bournel, C. Salzemann, C. Petit, J. J. Gallet and W. Q. Jie, *ACS Catal.*, 2019, **9**, 10212–10225.
27 S. Riyajuddin, K. Azmi, M. Pahuja, S. Kumar, T. Maruyama, C. Bera and K. Ghosh, *ACS Nano*, 2021, **15**, 5586–5599.
28 M. M. Guo, Y. X. Yuan, Y. H. Qu, T. Yu, C. L. Yuan and Z.-H. Lu, *Chem. Commun.*, 2022, **58**, 1597–1600.
29 D. Wang, Y. X. Chang, Y. R. Li, S. L. Zhang and S. L. Xu, *Rare Met.*, 2021, **40**, 3156–3165.
30 B. L. Deng, L. P. Guo, Y. Lu, H. B. Rong and D. C. Cheng, *Rare Met.*, 2022, 1–10.
31 Y. J. Li, W. Pei, J. T. He, K. Liu, W. H. Qi, X. H. Gao, S. Zhou, H. P. Xie, K. Yin, Y. L. Gao, J. He, J. J. Zhao, J. H. Hu, T.-S. Chan, Z. Li, G. F. Zhang and M. Liu, *ACS Catal.*, 2019, **9**, 10870–10875.
32 W. F. Zhai, Y. Chen, Y. D. Liu, T. Sakthivel, Y. Y. Ma, S. W. Guo, Y. Q. Qu and Z. F. Dai, *Adv. Funct. Mater.*, 2023, **33**, 2301565.
33 Y. X. Zhou, H. B. Yao, Y. Wang, H. L. Liu, M. R. Gao, P. K. Shen and S. H. Yu, *Chem. – Eur. J.*, 2010, **16**, 12000–12007.
34 T. T. Liang, Z. F. Dai, Y. D. Liu, X. Zhang and H. B. Zeng, *Sci. Bull.*, 2021, **66**, 2471–2478.
35 X. B. Zheng, Y. P. Chen, W. H. Lai, P. Li, C. L. Ye, N. N. Liu, S. X. Dou, H. G. Pan and W. P. Sun, *Adv. Funct. Mater.*, 2022, **32**, 2200663.
36 T. K. Das, T. Ping, M. Mohapatra, S. Anwar, C. S. Gopinath and B. K. Jena, *Chem. Commun.*, 2022, **58**, 3689–3692.
37 H. Y. Mou, Z. M. Xue, B. L. Zhang, X. Lan and T. C. Mu, *J. Mater. Chem. A*, 2021, **9**, 2099–2103.
38 X. Zhang, R. Y. Bi, J. Y. Wang, M. Zheng, J. Wang, R. B. Yu and D. Wang, *Adv. Mater.*, 2023, **35**, 2209354.
39 C. B. Sun, J. Ding, H. Z. Wang, J. Liu, X. P. Han, Y. D. Deng, C. Zhong and W. B. Hu, *J. Mater. Chem. A*, 2021, **9**, 13926–13935.
40 X. J. Hu, Y. F. Chen, M. R. Zhang, G. T. Fu, D. M. Sun, J. M. Lee and Y. W. Tang, *Carbon*, 2019, **144**, 557–566.
41 S. Mendioroz, J. A. Pajares, I. Benito, C. Pesquera, F. Gonzalez and C. Blanco, *Langmuir*, 1987, **3**, 676–681.
42 S. B. Wang, B. Y. Guan, X. Wang and D. Lou, *J. Am. Chem. Soc.*, 2018, **140**, 15145–15148.
43 P. Yu, L. Wang, F. F. Sun, Y. Xie, X. Liu, J. Y. Ma, X. W. Wang, C. G. Tian, J. H. Li and H. G. Fu, *Adv. Mater.*, 2019, **31**, 1901666.
44 H. B. Geng, J. Yang, Z. F. Dai, Y. Zhang, Y. Zheng, H. Yu, H. W. Wang, Z. Z. Luo, Y. Y. Guo, Y. F. Zhang, J. W. Zheng, Y. G. Yang, Q. Y. Yan and H. W. Gu, *Small*, 2017, **13**, 1603490.